THERMAL-HYDRAULIC ANALYSIS OF WATER BASED ZIRCONIUM OXIDE NANOFLUIDS IN SEGMENTAL BAFFLED SHELL AND TUBE HEAT EXCHANGERS

Muhammad SAJJAD [*1], Hassan ALI [2], Muhammad Sajid KAMRAN [2]

[*1] Department of Mechanical Engineering, Khwaja Fareed University of Engineering & Information Technology, Rahim Yar Khan 64200, Pakistan

[2] Faculty of Engineering, University of Engineering & Technology, Lahore 54890, Pakistan

[*] Corresponding author; E-mail: muhammad.sajjad@kfueit.edu.pk

Thermal-hydraulic characteristics of water based ZrO_2 nanofluids has been investigated in a segmental baffled shell and tube heat exchanger in turbulent flow regime. The effect of Reynolds number, nanoparticle loading, mass flow rate, and tube layout has been analysed on overall heat transfer coefficient. The effect of Reynolds number on the tube side pressure drop and convective heat coefficient have also been discussed. The effect of shell side mass flow rate was also investigated on shell side heat transfer coefficient determined using Bell-Delaware method. The nanoparticle volume concentration is taken very low i.e. 0.2%, 0.4% and, 0.8% respectively. The improvement in both tube side convective heat transfer coefficient and overall heat transfer coefficient has been observed. The maximum improvement in the convective heat transfer coefficient is found to be 14.1% for 0.8% ZrO_2 nanofluids. However, the percentage enhancement in tube side pressure drop was higher than the percentage increment in the tube side heat transfer coefficient.

Key words*: Nanofluids, Heat exchangers, Heat transfer coefficient, Pressure drop*

1. Introduction

Heat exchangers are one of the important potential applications of nanofluids. Nanofluids have acquired a lot of importance in a wide range of applications from last few decades. The nanomaterial, one of the important part of the nanofluid, can be obtained from multiple sources including metals, non-metals, metal oxide, and semiconductors. For example, the metal nanoparticles can be obtained from aluminium, copper and other metals, while metal oxide nanomaterials are obtained from aluminium oxide, titanium oxide, copper oxide, iron oxide and etc. The non-metal nanoparticles, for instance, includes single and multi-walled carbon nanotubes, graphene oxide, graphene nanoplatelets and nano-diamonds. The further details on various types of nanparticles, base fluids and nanomaterials along with their thermophysical properties and thermal-hydraulic characteristics can be found in recent review studies performed by Gupta et al. [1], Ganvir et al. [2], Leong et al. [3], and Ambreen and Kim [4].

Farajollahi et al. [5] analysed the heat transfer performance of water based aluminium oxide and titanium oxide nanofluids in a shell and tube heat exchanger. The effect of nanoparticle loading and

Peclet number was studied on different parameters such as tube side heat transfer coefficient, tube side Nusselt number, and overall heat transfer coefficient. They observed a maximum enhancement in overall heat transfer coefficient of 16% at a volume concentration of 0.75%, and at Peclet number of 50,000 for H_2O – Al_2O_3 nanofluids. The heat transfer enhancement using multi-walled carbon nanotubes as a nanomaterial was studied by Lotfi et al. [6] in a shell and tube heat exchanger. They observed an increase in the overall heat transfer coefficient with both nanoparticle volume concentrations and flow rate. Cox et al. [7] investigated the thermal performance of H_2O – SiO_2 nanofluids in shell and tube heat exchanger, considering the effect of mass flow rate on overall heat transfer coefficient. The maximum intensification in overall heat transfer coefficient was 9% at a weight concentration of 4% and at a mass flow rate of 950 kg/hr. Albadr et al. [8] also investigated the effect of mass flow rate and volume concentration on thermal characteristics of H_2O – Al_2O_3 nanofluids in a shell tube heat exchanger in the turbulent flow regime. The enhancement observed in the overall heat transfer coefficient, was 57% at a volume concentration of 2%.

Table 1 Summary of literature survey for the thermal performance of nanofluids in shell and tube heat exchangers

Author(s)	Nanofluids	Particle loading	Findings
Farajollahi et al. [5]	H_2O – Al_2O_3	ϕ_v = 0.3 - 2%	Highest enhancement in overall heat transfer coefficient for H_2O – γ-Al_2O_3 nanofluids was 16% at ϕ_v = 0.75% and Pe = 50,000 Highest enhancement in overall heat transfer coefficient for H_2O – TiO2 nanofluids was 24% at ϕ_v = 0.3% and Pe = 44,000
	H_2O – TiO_2	ϕ_v = 0.15 - 0.75%	
Cox et al. [7]	H_2O – SiO_2	ϕ_w = 2 - 6%	Maximum enhancement in total heat transfer coefficient was 9% at ϕ_w = 4% and m = 950 kg/hr
Albadr et al. [8]	H_2O – Al_2O_3	ϕ_v = 0.3 - 2%	Maximum enhancement in overall heat transfer coefficient was 57% at ϕ_v = 2% and Re = 180,349.123
Shahrul et al. [9]	H_2O – SiO_2	ϕ_v = 0.5%	12% enhancement in overall heat transfer coefficient for 0.5 vol.% H_2O – SiO_2 nanofluids, 26% for 0.5 vol.% H_2O – Al_2O_3 nanofluids, and 35% for 0.3 vol.% H_2O – ZnO nanofluids respectively.
	H_2O – Al_2O_3	ϕ_v = 0.5%	
	H_2O – ZnO	ϕ_v = 0.3%	
Akhtari et al. [10]	H_2O – Al_2O_3	ϕ_v = 0.2 – 0.5%	Enhancement in overall heat transfer coefficient was 23.9% at ϕ_v = 0.5% and base fluid flow rate of 90 l/hr
Kumar and Sonawane [11]	H_2O – Fe_2O_3 EG – Fe_2O_3	ϕ_v = 0.02 – 0.08%	Maximum enhancement of 20% for Fe_2O_3/H_2O nanofluids, and 13% for Fe_2O_3/EG nanofluids in convective heat transfer coefficient
Haque et al. [12]	H_2O – Al_2O_3	ϕ_m = 1 - 2%	Maximum improvement in convective heat transfer coefficient was 59.08 % for Al_2O_3 for 2 .wt% Al_2O_3 nanofluids

Akhtari et al. [10] carried experimental and computational fluid dynamics analysis to study the heat transfer characteristics of H_2O – Al_2O_3 nanofluids in a shell and tube, and in a double pipe heat exchanger. They found significant enhancement in heat transfer coefficient, up to 23.9% at a volume concentration of 0.5%. Shahrul et al. [13] analysed the effect of volume concentration on thermophysical properties, heat transfer coefficient, and energy effectiveness of various nanofluids in a shell and tube heat exchanger. The highest improvement in convective heat transfer coefficient was 14.29 %, 12.89 %, 10.10 %, 9.86 %, 9.76 % and 2.18 % for Al_2O_3, Fe_3O_4, TiO_2, ZnO, CuO and SiO_2 nanofluids respectively, at a volume concentration of 0.3% and a mass flow rate of 50 kg/min for both shell side and tube side fluid. Kumar and Sonawane [11] experimentally measured the heat

transfer performance of nanofluids, prepared by suspending Fe_2O_3 nanoparticles in two types of base fluids i.e. water and ethylene glycol. They observed a 20% improvement in the convective heat transfer coefficient for Fe_2O_3/H_2O nanofluids and 13% for Fe_2O_3/EG nanofluids. Shahrul et al. [9] experimentally evaluated the performance of three types of nanofluids: H_2O – Al_2O_3, H_2O – SiO_2 and H_2O – ZnO. They found 12% enhancement in overall heat transfer coefficient for 0.5 vol.% H_2O – SiO_2 nanofluids, 26% for 0.5 vol.% H_2O – Al_2O_3 nanofluids, and 35% for 0.3 vol.% H_2O – ZnO nanofluids respectively. Heydari et al. [14] performed simulations to measure the heat transfer coefficient and heat transfer rate of a number of nanofluids using water and ethylene glycol as a base fluid and taking Al_2O_3, Fe_2O_3, SiO_2, Au, Fe, CuO and Cu as nanoparticles with volume concentrations of 1-5%. The observed that the heat transfer coefficient decreases with the increase in volume concentration for all types of nanofluids. Haque et al. [12] experimentally found maximum enhancement of 35.82% and 59.08% in heat transfer rate and heat transfer coefficient respectively, for 2 wt.% H_2O-Al_2O_3 nanofluids, in a vertical shell and tube heat exchanger. The summary of these important studies can be found in Table 1. It can be observed from the literature survey that the nanofluids containing ZrO_2 nanoparticles have not extensively been studied in shell and tube heat exchangers. Therefore, the current study investigates the thermal-hydraulic characteristics of water based ZrO_2 nanofluids in a segmental baffled shell and tube heat exchanger.

2. Heat exchanger specifications

The shell and tube heat exchanger consists of 48 tubes, with an inner and outer diameter of 0.005 m and 0.006 m respectively. The shell inside and outside diameter are 0.071 m and 0.0748 m respectively. The tubes are made of brass, and a shell of stainless steel. The heat exchanger consists of three segmental baffles with baffle cut of 30%. The length of the tubes is taken 0.202 m and tube layout is 30° unless specified. The hot and cold fluids (i.e nanofluid) were taken on the shell side and tubes side respectively.

3. Thermophysical properties of nanofluids

The thermophysical properties of the base fluid and the nanofluids were evaluated at mean temperature for further calculations. The viscosity, thermal conductivity, specific heat capacity and density of water was determined by the correlations of Popiel and Wojtkowiak [15]. The thermophysical properties of ZrO_2 nanofluids were determined, employing Eqs. (1) and (4) [16]. The density and specific heat capacity of ZrO_2 nanoparticle were considered 5,570 kg/m^{3}and 480 kJ/kg K respectively [17].

$$\rho_{\mathrm{nf}} = \phi_v \rho_{nm} + (1-\phi_v)\rho_{bf} \tag{1}$$

$$\rho_{nf} C_{p,nf} = \phi_v \rho_{nm} C_{p,nm} + (1-\phi_v)\rho_{bf} C_{p,bf} \tag{2}$$

$$\mu_{\mathrm{nf}} = \mu_{\mathrm{bf}} (550.82\phi_v^{\,2} + 46.801\phi_{\mathrm{v}} + 1) \tag{3}$$

$$k_{nf} = k_{bf} (-29.867\phi_v^{\,2} + 2.4505\phi_{\mathrm{v}} + 1) \tag{4}$$

4. Theoretical modeling

There are different correlations to determine the tube side Nusselt number of nanofluids such as Xuan and Li correlation [18], Gnielinski correlation [5], and Dittus–Boelter correlation [19]. Xuan and Li correlation is only applicable at very low nanoparticle loadings, and it generally over predicts Nusselt number as investigated by Farajollahi et al. [5]. Kumar and Sonawane [11] concluded that Gnielinski correlation provides more accurate results as compared to both Dittus–Boelter and Xuan and Li correlation. Therefore, in the current study, Gnielinski correlation for turbulent flow, given by Eq. (5), was employed for the investigation of the tube side Nusselt number. The tube side Darcy friction factor was calculated using Blasius correlation [11] as given by Eq. (7).

$$Nu_t = 0.012(\mathrm{Re}_t^{0.87} - 280)\,\mathrm{Pr}_t^{0.4} \tag{5}$$

$$h_t = \frac{Nu_t k_t}{D_i} \tag{6}$$

$$f_t = 0.316\,\mathrm{Re}_t^{(-1/4)} \tag{7}$$

$$\Delta Pt = \left(f_t \frac{NpL}{2D_i} \right) \rho_t u_t^{\,2} \tag{8}$$

The Bell Delaware method was employed for the calculation of shell side heat transfer coefficient as it is more accurate than other theoretical methods such as Kern and Wills-Johnston methods as discussed by Abdelkader and Zubair [20]. The Eq. (9) provides heat transfer coefficient on the shells side. The ideal tube bank heat transfer coefficient, h_i, was calculated by Eq. (10), while the values of correlation coefficients a_1, a_3 and a_4 were taken from Wolverine [21]. The unequal baffle spacing correction factor, J_s, was determined using Eq. (11); where n is equal to 0.6 and 1/3 for turbulent flow and laminar flow respectively.

$$h_s = h_i[J_s J_B J_c J_\mu J_R J_L] \tag{9}$$

$$h_i = \left(a_1 \left(\frac{1.33 D_i}{Lt} \right)^{\frac{a_3}{1+0.14\,\mathrm{Re}^{a_4}}} \right) \frac{j_i CpG}{\mathrm{Pr}^{-2/3}} \tag{10}$$

$$J_s = \left(\frac{(Nb-1) + c_1^{\,1-n} + c_2^{\,1-n}}{(Nb-1) + c_1 + c_2} \right),\ c_1 = \frac{Lbi}{Lbc} \text{ and } c_2 = \frac{Lbo}{Lbc} \tag{11}$$

The bundle bypass correction factor of the tube, J_B, was calculated using Eq. (12). The value of C_{bh} is taken 1.25 and 1.35 for turbulent and laminar flow respectively.

$$J_B = \exp\left[-C_{bh} \frac{L_{bc}[D_s - D_{otl}] + L_{pl}}{S_m} (1 - \sqrt[3]{2r_{ss}}) \right] \tag{12}$$

$$r_{ss} = \frac{N_{ss}}{D_s / L_{pp}[1 - 2(B_c/100)]} \tag{13}$$

The baffle cut correction factor, J_C, was determined using Eq. (14). The wall viscosity correction factor is determined using Eq. (16). The laminar flow correction factor is given by Eq. (17).

$$Jc = 0.55 + 0.72\left[1 - 2\left(\frac{\theta_{ctl}}{360} - \frac{Sin\theta_{ctl}}{2\pi}\right)\right] \quad (14)$$

$$\theta_{ctl} = 2\cos^{-1}\left[\left(\frac{D_s}{D_{ctl}}\right)\right]\left(1 - \frac{2B_c}{100}\right) \quad (15)$$

$$J_\mu = \left[\frac{\mu}{\mu_w}\right]^{0.14} \quad (16)$$

$$J_R = \left(\frac{10}{N_c}\right)^{0.18} + \left[\left(\frac{10}{N_c}\right)^{0.18} - 1\right]\left(\frac{20 - \mathrm{Re}}{80}\right) \quad (17)$$

$$\text{Where, } N_c = \left\{\left[N_{tcc} + \frac{0.8}{L_{pp}}\left[D_s\left(\frac{B_c}{100}\right) - \frac{(D_s - D_{ctl}}{2}\right]\right]\right\}(N_b + 1) \quad (18)$$

The baffle leakage correction factor, J_L, was calculated using Eq. (19).

$$J_L = 0.44(1 - r_s) + (1 - 0.44(1 - r_s))e^{-2.2r_{lm}} \quad (19)$$

$$\text{Where, } r_s = \frac{S_{sb}}{S_{sb} + S_{tb}},\ r_{lm} = \frac{S_{sb} + S_{tb}}{S_m},\ S_{sb} = 0.00436 D_s L_{sb} \quad (20)$$

$$S_{tb} = \left[\frac{\pi}{4}(D_t + L_{tb})^2\right] N_t (1 - F_w) \quad (21)$$

$$S_m = L_{bc}\left[L_{bb} + \frac{D_{ctl}}{P_{T,e}}(P_T - D_t)\right] \quad (22)$$

$$\theta_{ds} = 2\cos^{-1}\left[1 - 2\left(\frac{B_c}{100}\right)\right] \quad (23)$$

The overall heat transfer coefficient for the heat exchanger was determined using Eq. (24).

$$\frac{1}{U} = \frac{1}{h_s} + D_i\frac{\ln\left(\frac{D_o}{D_i}\right)}{2k_t} + \frac{D_i}{D_o}\left(\frac{1}{h_t}\right) \quad (24)$$

4.1. Validation of theoretical model

The theoretical model for the evaluation of thermohydraulic characteristics of ZrO_2 nanofluids, was validated by finding the overall heat transfer coefficient and pressure drop of the water. The shell side heat transfer coefficient was determined using Bell-Delaware method and tube side heat transfer was calculated using Gnielinski correlation. The results for the overall heat transfer coefficient were compared with the experimental investigation of Barzegarian et al. [22]. The variation

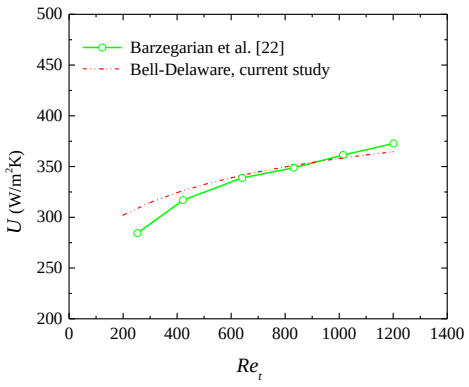

Fig. 1 Comparison of the overall heat transfer coefficient with the corresponding experimental results, at a shell side mass flow rate of 4.4 kg/min

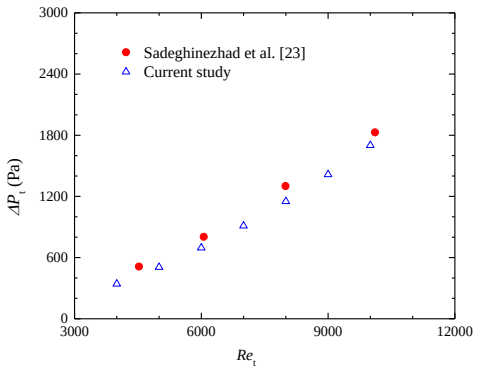

Fig. 2 Comparison of the pressure drop with the corresponding investigations of Sadeghinezhad et al. [23]

in overall heat transfer coefficient with Reynolds number is shown in Fig. 1. The analysis of the Fig. 1 reveals that the results of Bell-Delaware method are in good agreement with the experimental results, as the maximum deviation is under 10%. So, the Bell-Delaware method can be used for the investigation of thermohydraulic characteristics of nanofluids. The validation for the pressure drop is shown in Fig. 2. The comparison shows that the results of the current study are in good agreement with the corresponding results of Sadeghinezhad et al. [23].

5. Results

5.1. Tube side heat transfer coefficient

The influence of Reynolds number over the tube side heat transfer coefficient is indicated in Fig. 3. The heat transfer coefficient has an increasing trend for all volume concentrations and a similar trend was as observed by Shahrul et al. [9] for water based ZnO, SiO_2 and Al_2O_3 nanofluids. The increasing rates of heat transfer coefficient are 0.807, 0.837, 0.865, 0.922 at nanoparticle concentrations of 0%, 0.2%, 0.4% and 0.8% respectively. A uniform augmentation in heat transfer

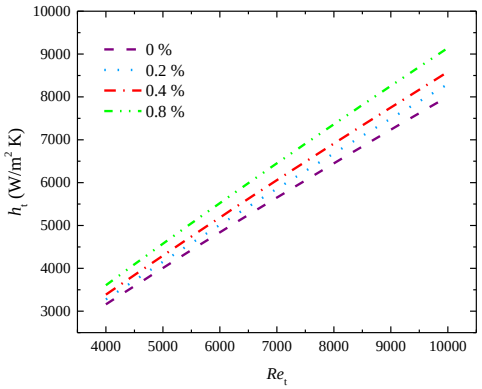

Fig. 3 Tube side convective heat transfer coefficient versus tube side Reynolds number for ZrO_2 nanofluids

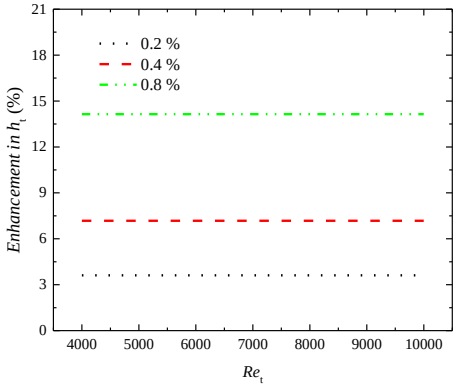

Fig. 4 Enhancement in tube side convective heat transfer coefficient with tube side Reynolds number

coefficient was predicted for Reynolds number of Re = 4,000 - 10,000 at all nanoparticle concentrations. The inclusive analysis of the Fig. 4. indicates that there is 3.6 % increment for 0.2% ZrO_2 nanofluids, 7.2% for 0.4% ZrO_2 nanofluids, and 14.1% for 0.8% ZrO_2 nanofluids respectively at all Reynolds numbers. This higher heat transfer coefficient of nanofluids is perhaps due to the higher thermal conductivity of ZrO_2 nanoparticles than that of water. The experimental investigations carried by Farajollahi et al. [5] revealed that there was a 46% improvement in convective heat transfer coefficient for alumina nanofluids and 56% for titina nanofluids at a volume concentration of 0.3% for both fluids. Kumar and Sonawane [11] found maximum enhancement of 20% for Fe_2O_3/H_2O nanofluids, and 13% for Fe_2O_3/EG nanofluids at a discharge of 3 L/min. However, in this case, the percentage augmentation in tube side convective heat transfer coefficient of ZrO_2 nanofluids is much lower than both the Al_2O_3/H_2O and TiO_2/ H_2O nanofluids.

5.2. Tube side pressure drop

The tube side pressure drop of the nanofluids was calculated by considering the effects of Reynolds number and particle concentration. Also, the analysis of the heat transfer intensification using nanofluids is incomplete if the effects of enhanced viscosity of the nanofluids are not taken into account. The increased viscosity of the nanofluids results in more pressure drop, and this fact can be clearly seen in Fig. 5. The pressure drop is 480.8 Pa at Re = 4,000 and, 2,390 Pa at Re = 10,000 for volume concentration of 0.4%. Likewise, pressure drop is 911.51 Pa for 0% nanofluids, and 1747.1 Pa for 0.8% nanofluids at Reynolds number of 7,000. As far as percentage enhancement in pressure drop is concerned, it increases with the increase in volume concentration but suffers insignificant variation with Reynolds number as given by Fig. 6. For instance, the increase in pressure drop was 18.9%, 40.5% and 91.6% at volume concentration of 0.2%, 0.4% and 0.8% respectively, and at a Reynolds number of 4,000.

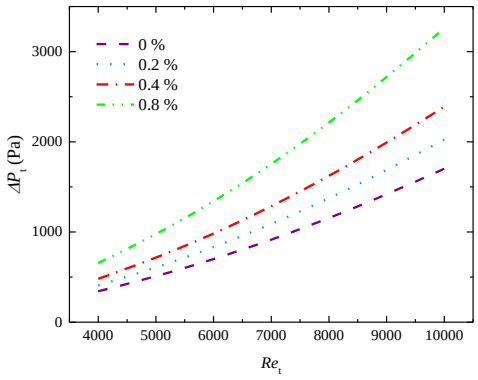

Fig. 5 Tube side pressure drop versus tube side Reynolds number

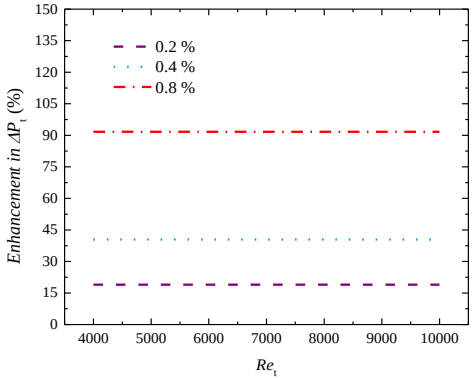

Fig. 6 Enhancement in tube side pressure drop versus tube side Reynolds number

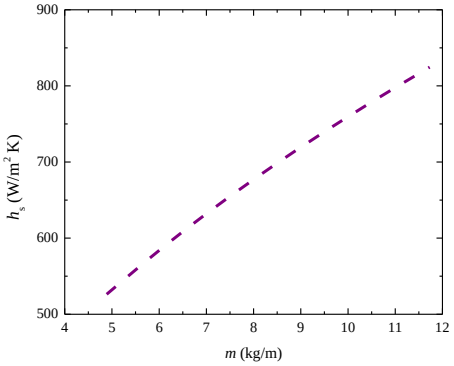

Fig. 7 Shell side heat transfer coefficient versus shell side mass flow rate for water

5.3 Shell side heat transfer coefficient

The shell side heat transfer coefficient of the water was calculated using Bell-Delaware method. The Fig. 7 depicts the effect of shell side mass flow rate on shell side heat transfer coefficient. It is obvious from Fig. 7 that the mass flow rate has a positive effect on the shell side heat transfer coefficient, and it increases with the enhancement in shell side mass flow rate. The shell side heat transfer coefficient

increased 526.3 to 824.8 W/m^2 K when the shell side mass flow rate was increased from 4.9 kg/min to 11.7 kg/min respectively, as shown in Fig. 7.

5.3. Overall heat transfer coefficient

Fig. 8 to Fig. 10 represents the dependence of overall heat transfer coefficient of H_2O – ZrO_2 nanofluids on different factors such as tube side Reynolds number, shell side mass flow rate, and the tubes' configuration. The overall heat transfer coefficient increases with the increase in tube side Reynolds number, for instance, it increased from 463.2 W/m^2 K (Re = 4,000) to 498.8 W/m^2 K (Re = 10,000) for volume concentration of 0.2%.

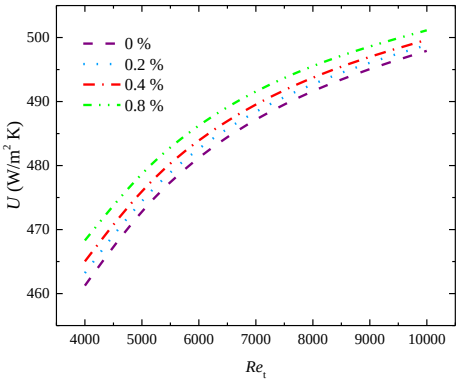

Fig. 8 Overall heat transfer coefficient versus tube side Reynolds number for ZrO_2 nanofluids

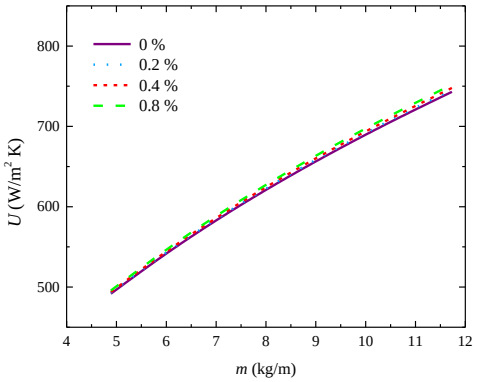

Fig. 9 Overall heat transfer coefficient versus shell side mass flow rate for ZrO_2 nanofluid

In the same way, the overall heat transfer coefficient increases with the increase in volume concentration, for example, overall heat transfer coefficient was 483 W/m^2 K for 0.2% H_2O – ZrO_2 nanofluids and it increased to 486.6 W/m^2 K for 0.8% H_2O – ZrO_2 nanofluids at Reynolds number of 6000. However, it is important to note that the augmentation in overall heat transfer coefficient decreases with the increase in Reynolds number as revealed in Fig. 10. So, it is clear that the overall heat transfer coefficient is higher on the lesser tube side Reynolds numbers. Likewise, the overall heat transfer coefficient was determined at different volume concentrations and its variation with the shell side mass flow rate was studied. The overall heat transfer coefficient also increases with the increase in shell side mass flow rate as shown in Fig. 10. However, there is no significant improvement in overall heat transfer coefficient with the volume concentration, particularly at a lesser shell side mass flow rate.

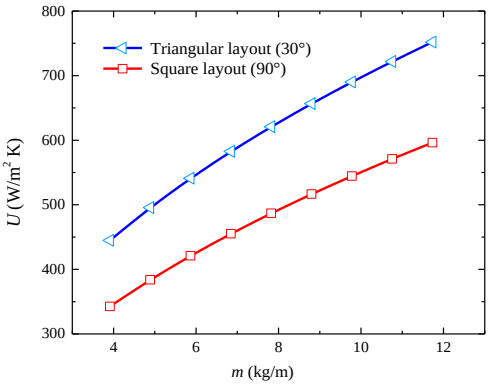

Fig. 10 Overall heat transfer coefficient for different tube layouts

The influence of the tube arrangements on the overall heat transfer coefficient was analysed for 0.8% ZrO_2 nanofluids as depicted in Fig. 10. The overall heat transfer coefficient provided by the triangular layout (30°) is larger than that of the square layout (90°). For instance, the overall heat

transfer coefficient using triangular tube layout was 27% more than that of square layout at the shell side mass flow rate of 7.8 kg/m and tube side Reynolds number of 8,000 for volume concentration of 0.8%. Although the triangular layout provides a higher heat transfer coefficient, it accompanies with some challenges associated with the cleaning of the heat exchanger tubes.

5.4. Comparison with other nanofluids

The thermal performance of H_2O – ZrO_2 nanofluids as compared to nanofluids containing Al_2O_3, TiO_2, SiO_2 and ZnO nanoparticles is lower. For example, Farajollahi et al. [5] observed enhancement in overall heat transfer coefficient for H_2O – γ-Al_2O_3 and H_2O – TiO_2 nanofluids up to 16% and 24% at ϕ_v = 0.75% and ϕ_v = 0.3% respectively, while in the present case, the highest enhancement is 14.1% for 0.8% volume concentration for H_2O – ZrO_2 nanofluids. Similarly 12% enhancement in overall heat transfer coefficient for 0.5 vol.% H_2O – SiO_2 nanofluids, 26% for 0.5 vol.% H_2O – Al_2O_3 nanofluids, and 35% for 0.3 vol.% H_2O – ZnO nanofluids respectively observed by Shahrul et al. [9] indicates the superiority of H_2O – Al_2O_3 and H_2O – ZnO nanofluids over H_2O – ZrO_2 nanofluids. It may be due to the better thermophysical properties of H_2O – Al_2O_3 and H_2O – ZnO nanofluids as compared to H_2O – ZrO_2 nanofluids. It means H_2O – ZrO_2 nanofluids are not as effective as other conventional nanofluids in heat transfer applications.

6. Conclusion

The thermohydraulic characteristics of zirconium oxide nanofluids at low volume concentrations in a segmental baffled shell and tube heat exchanger were investigated. The effect of tube side Reynolds number was studied on tube side convective heat transfer coefficient and overall heat transfer coefficient. An improvement in tube side heat transfer coefficient was found. The convective heat transfer coefficient of the tube was increased by 3.6 % for 0.2% ZrO_2 nanofluids, 7.2% for 0.4% ZrO_2 nanofluids, and 14.1% for 0.8% ZrO_2 nanofluids respectively. The overall heat transfer coefficient was increased with the increase in tube side Reynolds number, shell side mass flow rate and volume concentrations. However, the effect of volume concentration was less, when the variation in overall heat transfer coefficient was analysed with the shell side mass flow rate. The triangular tube configuration provided the higher heat transfer coefficient than square tube configuration. The percentage increase in tube side pressure drop was higher as compared to percentage augmentation in tube side heat transfer coefficient. This shows that the improved heat transfer characteristics of water based ZrO_2 nanofluids are accompanied with the penalty of enhanced pressure drop.

Nomenclature

B_c	– baffle cut, [-]	D_s	– shell inside diameter, [m]
C_{bh}	– empirical factor, [-]	D_t	– tube outside diameter, [m]
Cp	– specific heat, [kJkg^{-1}K^{-1}]	ΔP_t	– tube side pressure drop, [Pa]
D_{ctl}	– tube center limit diameter, [m]	f	– friction factor, [-]
D_i	– tube inside diameter, [m]	G	– mass flux, [kgs−1m−2]
D_{otl}	– tube outside limit diameter, [m]	h_i	– ideal tube bank heat transfer coefficient,

[Wm^{-2} K^{-1}]

h_s – shell side heat transfer coefficient, [Wm^{-2} K^{-1}]

h_t – tube side heat transfer coefficient, [Wm^{-2} K^{-1}]

J_B – bundle bypass correction factor, [-]

J_C – baffle cut correction factor, [-]

J_L – baffle leakage correction factor, [-]

J_μ – wall viscosity correction factor, [-]

J_R – laminar flow correction factor, [-]

J_s – unequal baffle spacing correction factor, [-]

k – thermal conductivity, [$Wm^{-1}K^{-1}$]

L – length of tubes, [m]

L_{bi} – inlet baffle spacing, [m]

L_{bb} – bypass channel clearance, [m]

L_{bc} – central baffle spacing, [m]

L_{bo} – outlet baffle spacing, [m]

L_{pl} – tubes bypass lane width, [m]

L_{sb} – diametral clearance (shell to baffle), [m]

m – mass flow rate, [kgs^{-1}]

N_b – number of baffles, [-]

N_c – number of tube rows, [-]

N_p – number of passes, [-]

N_{ss} – sealing strips quantity, [-]

N_{tc} – number of tube rows per baffle section (crossed between baffle tips), [-]

N_{ut} – tube side Nusselt number, [-]

Pe – Peclet number, [-]

Pr – Prandtl number, [-]

P_T – tube pitch, [m]

$P_{t,e}$ – effective tube pitch, [m]

Re – Reynolds number, [-]

r_s – ratio of areas, [-]

r_{ss} – ratio of sealing strips quantity and number of tubes in one baffle section, [-]

S_m – cross flow area of tubes at center line, [m^2]

S_{sb} – shell to baffle leakage area, [m^2]

S_{tb} – tube to baffle leakage area, [m^2]

θ_{ctl} – baffle cut angle (relative to centerline) in degrees, [-]

θ_{ds} – baffle cut angle in degrees, [-]

U – overall heat transfer coefficient, [Wm^2K^{-1}]

u – average velocity of fluid, [ms^{-1}]

Subscripts

bf – base fluid

m – mass concentration

nf – nanofluid

nm – nanoparticle

s – shell

t – tube

v – volume concentration

w – wall

Greek symbols

ϕ – nanoparticle concentration, [-]

ρ – density of fluid, [kg m^{-3}]

μ – viscosity, [Pa s]

References

[1] Gupta, M., et. al., A Review on Thermophysical Properties of Nanofluids and Heat Transfer Applications, *Renewable and Sustainable Energy Reviews, 74* (2017), pp. 638-670

[2] Ganvir, R. B., et. al., Heat Transfer Characteristics in Nanofluid—A Review, *Renewable and Sustainable Energy Reviews, 75* (2017), pp. 451-460

[3] Leong, K. Y., et. al., Synthesis and Thermal Conductivity Characteristic of Hybrid Nanofluids – A Review, *Renewable and Sustainable Energy Reviews, 75* (2017), pp. 868-878

[4] Ambreen, T., Kim, M.-H., Heat Transfer and Pressure Drop Correlations of Nanofluids: A State of Art Review, *Renewable and Sustainable Energy Reviews, 91* (2018), pp. 564-583

[5] Farajollahi, B., et. al., Heat Transfer of Nanofluids in a Shell and Tube Heat Exchanger, *International Journal of Heat and Mass Transfer, 53* (2010), 1–3, pp. 12-17

[6] Lotfi, R., et. al., Experimental Study on the Heat Transfer Enhancement of MWNT-Water Nanofluid in a Shell and Tube Heat Exchanger, *International Communications in Heat and Mass Transfer, 39* (2012), 1, pp. 108-111

[7] Cox, J., et. al., Application of Nanofluids in a Shell-and-Tube Heat Exchanger, *Proceedings*, ASME 2013 11th International Conference on Nanochannels, Microchannels, and Minichannels, Sapporo, Japan, 2013, pp. V001T02A003

[8] Albadr, J., et. al., Heat Transfer Through Heat Exchanger Using Al2O3 Nanofluid at Different Concentrations, *Case Studies in Thermal Engineering, 1* (2013), 1, pp. 38-44
[9] Shahrul, I. M., et. al., Experimental investigation on Al2O3–W, SiO2–W and ZnO–W nanofluids and their application in a shell and tube heat exchanger, *International Journal of Heat and Mass Transfer, 97* (2016), pp. 547-558
[10] Akhtari, M., et. al., Numerical and Experimental Investigation of Heat Transfer of α-Al2O3/Water Nanofluid in Double Pipe and Shell and Tube Heat Exchangers, *Numerical Heat Transfer, Part A: Applications, 63* (2013), pp. 941-958
[11] Kumar, N., Sonawane, S. S., Experimental Study of Fe2O3/Water and Fe2O3/Ethylene Glycol Nanofluid Heat Transfer Enhancement in a Shell and Tube Heat Exchanger, *International Communications in Heat and Mass Transfer, 78* (2016), pp. 277-284
[12] Haque, A. K. M. M., et. al., Forced Convective Heat Transfer of Aqueous Al_2O_3 Nanofluid Through Shell and Tube Heat Exchanger, *Journal of nanoscience and nanotechnology, 18* (2018), pp. 1730-1740
[13] Shahrul, I. M., et. al., Performance Evaluation of a Shell and Tube Heat Exchanger Operated With Oxide Based Nanofluids, *Heat and Mass Transfer, 52* (2016), 8, pp. 1425-1433
[14] Heydari, A., et. al., Numerical Analysis of a Small Size Baffled Shell and-Tube Heat Exchanger Using Different Nanofluids, *Heat Transfer Engineering*, (2017)
[15] Popiel, C. O., Wojtkowiak, J., Simple Formulas for Thermophysical Properties of Liquid Water for Heat Transfer Calculations (from 0°C to 150°C), *Heat Transfer Engineering, 19* (1998), 3, pp. 87-101
[16] Rea, U., et. al., Laminar Convective Heat Transfer and Viscous Pressure Loss of Alumina–Water and Zirconia–water nanofluids, *International Journal of Heat and Mass Transfer, 52* (2009), 7-8, pp. 2042-2048
[17] Li, X., et. al., A Parametric Study of the Heat Flux Partitioning Model for Nucleate Boiling of Nanofluids, *International Journal of Thermal Sciences, 98* (2015), pp. 42-50
[18] Xuan, Y., Li, Q., Heat Transfer Enhancement of Nanofluids, *International Journal of Heat and Fluid Flow, 21* (2000), 1, pp. 58-64
[19] Dittus, F. W., Boelter, L. M. K., Heat Transfer in Automobile Radiators of the Tubular Type, *International Communications in Heat and Mass Transfer, 12* (1985), 1, pp. 3-22
[20] Abdelkader, B. A., Zubair, S. M., The Effect of a Number of Baffles on the Performance of Shell-and-Tube Heat Exchangers, *Heat Transfer Engineering*, (2017) pp. 1-14
[21] Wolverine, *Wolverine Tube Heat Transfer Data Book*, Wolverine Tube Inc., Decatur, Georgia, 1984.
[22] Barzegarian, R., et. al., Thermal Performance Augmentation Using Water Based Al2O3-gamma Nanofluid in a Horizontal Shell and Tube Heat Exchanger Under Forced Circulation, *International Communications in Heat and Mass Transfer, 86* (2017), pp. 52-59
[23] Sadeghinezhad E., et. al., An Experimental and Numerical Investigation of Heat Transfer Enhancement for Graphene Nanoplatelets Nanofluids in Turbulent Flow Conditions, *International Journal of Heat and Mass Transfer, 81* (2015), pp. 41-51